MOLECULAR METABOLISM

Non-canonical NRF2 activation promotes a pro-diabetic shift in hepatic glucose metabolism

Pengfei Liu [1,6], Matthew Dodson [1,6], Hui Li [1], Cody J. Schmidlin [1], Aryatara Shakya [1], Yongyi Wei [1], Joe G.N. Garcia [2], Eli Chapman [1], Pawel R. Kiela [1,3], Qing-Yu Zhang [1], Eileen White [4], Xinxin Ding [1], Aikseng Ooi [1,**], Donna D. Zhang [1,5,*]

ABSTRACT

Objective: NRF2, a transcription factor that regulates cellular redox and metabolic homeostasis, plays a dual role in human disease. While it is well known that canonical intermittent NRF2 activation protects against diabetes-induced tissue damage, little is known regarding the effects of prolonged non-canonical NRF2 activation in diabetes. The goal of this study was to determine the role and mechanisms of prolonged NRF2 activation in arsenic diabetogenicity.

Methods: To test this, we utilized an integrated transcriptomic and metabolomic approach to assess diabetogenic changes in the livers of wild type, $Nrf2^{-/-}$, $p62^{-/-}$, or $Nrf2^{-/-}$; $p62^{-/-}$ mice exposed to arsenic in the drinking water for 20 weeks.

Results: In contrast to canonical oxidative/electrophilic activation, prolonged non-canonical NRF2 activation via p62-mediated sequestration of KEAP1 increases carbohydrate flux through the polyol pathway, resulting in a pro-diabetic shift in glucose homeostasis. This p62- and NRF2-dependent increase in liver fructose metabolism and gluconeogenesis occurs through the upregulation of four novel NRF2 target genes, ketohexokinase (*Khk*), sorbitol dehydrogenase (*Sord*), triokinase/FMN cyclase (*Tkfc*), and hepatocyte nuclear factor 4 (*Hnf4A*).

Conclusion: We demonstrate that NRF2 and p62 are essential for arsenic-mediated insulin resistance and glucose intolerance, revealing a pro-diabetic role for prolonged NRF2 activation in arsenic diabetogenesis.

1. INTRODUCTION

NRF2 is a transcription factor that regulates cellular redox and metabolic homeostasis and plays an important role in human disease. NRF2 regulates the expression of genes bearing an antioxidant response element (ARE) in their regulatory regions. NRF2 target genes have been shown to regulate nearly every facet of cellular function, including redox homeostasis, energy metabolism, protein quality control, and ultimately cell survival [1,2]. Despite being ubiquitously expressed, the basal level of NRF2 is normally kept low by KEAP1-CUL3-RBX1-mediated ubiquitylation and subsequent 26S proteasomal degradation. However, during stress, NRF2 is primarily activated via one of two mechanisms: (1) canonical KEAP1 cysteine-dependent activation or (2) non-canonical p62-dependent activation. During canonical NRF2 activation, KEAP1-Cys151 is modified, preventing NRF2 ubiquitylation and increasing the level of NRF2 and its downstream genes to protect cells from xenobiotic insults [3,4]. Once cellular homeostasis is restored, NRF2 returns to a low basal level, ensuring transient NRF2 upregulation [5]. In contrast, we also discovered that NRF2 can be activated in a SQSTM1/p62-KEAP1-dependent but Cys151-independent manner during autophagy dysregulation. Blockage of autophagosome-lysosome fusion leads to p62-mediated sequestration of KEAP1 into autophagosomes, preventing NRF2 ubiquitylation and degradation [6]. This non-canonical mode of activation leads to prolonged upregulation of NRF2 and ARE-containing target genes, conferring a cellular survival advantage and promoting metabolic reprogramming. Interestingly, we discovered that arsenic, a globally relevant environmental toxicant, carcinogen, and diabetogen, induces prolonged NRF2 activation through this non-canonical mechanism [7,8].

Canonical or non-canonical activation of NRF2 dictates its dual role in disease [9]. Pioneering research in the field previously demonstrated that canonical and intermittent NRF2 activation by chemopreventive compounds can prevent cancer initiation [10]; however, since our proposal of a "dark side" role for NRF2 in cancer in 2008 [11], our

Brief Communication

Figure 1: A non-canonical model of NRF2 diabetogenesis. (A) Schematic of the treatment regime and experimental workflow. (B–D) Body weight (g), glucose tolerance test, and insulin tolerance test in the 20-week-old WT, $Nrf2^{-/-}$, $p62^{-/-}$, and $Nrf2^{-/-};p62^{-/-}$ arsenic-treated mice compared to controls. (E) Area under the curve in panel C. (F) Serum insulin levels of the indicated genotypes following 20 weeks of arsenic treatment. Data = mean ± SD (n = 5). *p < 0.05 compared to controls.

team and others have provided convincing evidence that prolonged/uncontrolled NRF2 activation is a driver of cancer progression, metastasis, and resistance to therapy. NRF2 is highly expressed in many cancer types, and elevated NRF2 levels strongly correlate with tumor resistance to chemotherapy, increased recurrence, and a poorer prognosis [2,12]. While the "dark side" of NRF2 in cancer continues to emerge, very little is known regarding chronic non-canonical activation of NRF2 in the pathogenesis of other diseases, including diabetes. The increased prevalence of type II diabetes continues to represent a global health crisis. Similar to other metabolic diseases, genetics, sedentary lifestyle, age, diet, and environmental toxicant exposure represent the main risk factors associated with developing type II diabetes [13,14]. In particular, chronic

exposure to a wide array of environmental diabetogens, such as arsenic, has been shown to affect insulin production/sensitivity, blood sugar levels, and lipid profiles, all of which are common features of diabetes onset and progression [13,15]. As such, determining the tissue-specific metabolic profiles associated with diabetic outcomes as well as the molecular changes that drive these pathogenic metabolic shifts represents a critical need in the field.

In this study, we hypothesized that prolonged non-canonical activation of the NRF2 signaling cascade could be a key factor in driving the onset of key diabetic phenotypes. To test this, we used a chronic arsenic-induced type II diabetes mouse model as (1) human epidemiological studies have associated populations living in high arsenic-contaminated areas with a higher prevalence of type II diabetes
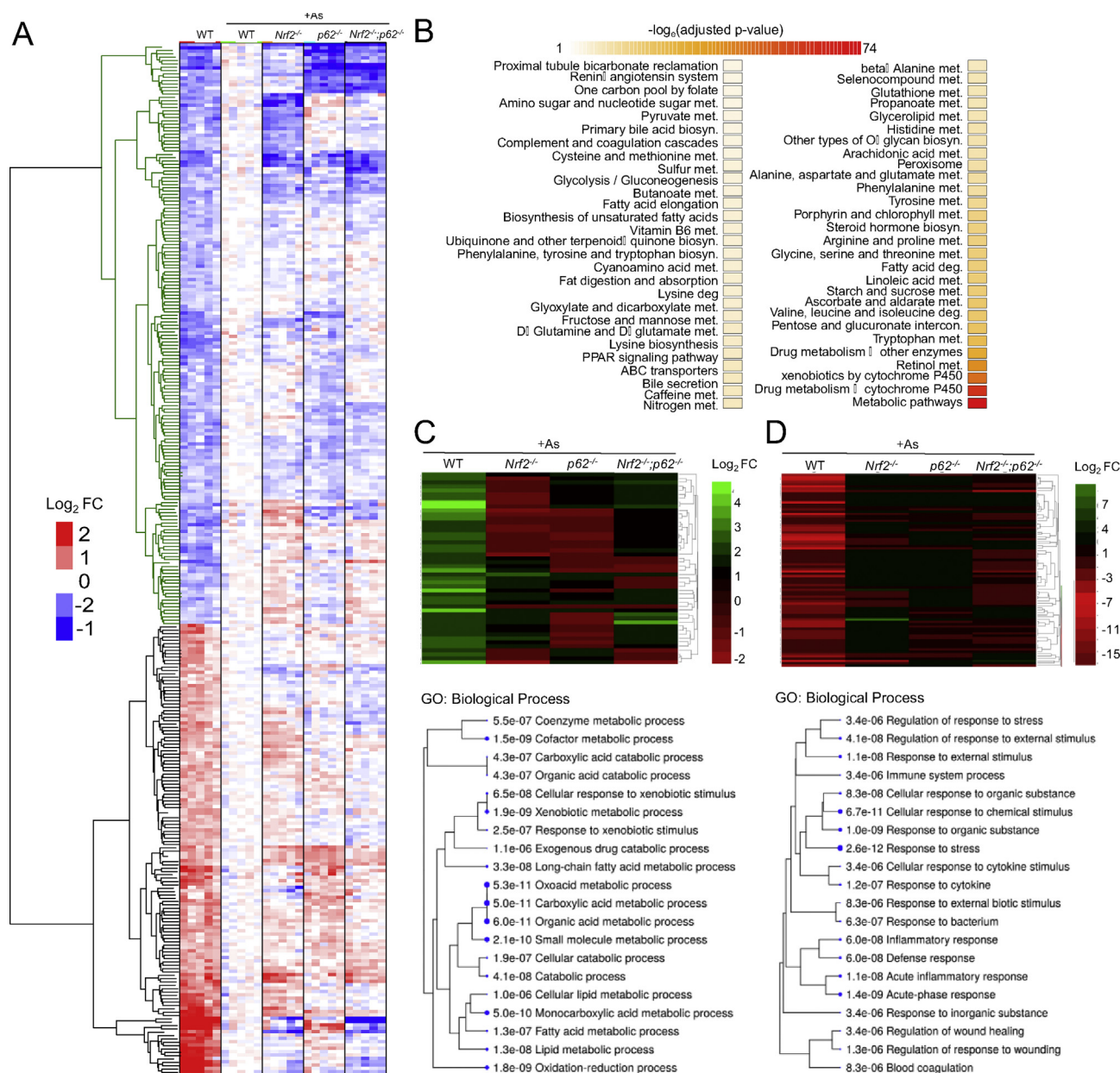
Figure 2: Non-canonical activation of NRF2 drove arsenic-induced transcriptomic changes. Liver tissue from the control or arsenic-exposed WT, *Nrf2*$^{-/-}$, *p62*$^{-/-}$, and *Nrf2*$^{-/-}$;*p62*$^{-/-}$ mice was assessed for changes in the transcriptome via RNAseq. (A) Heatmap indicating log2 fold change of significantly altered transcripts across the indicated genotypes compared to controls. (B) KEGG pathway analysis of metabolic pathways enhanced by arsenic exposure. (C) Heatmap indicating transcripts were significantly increased by arsenic in a p62-NRF2-dependent manner. Gene ontology (GO) enrichment analysis of biological processes enhanced by arsenic exposure in the WT mice. (D) Heatmap indicating transcripts were significantly decreased by arsenic in a p62-NRF2-dependent manner. Gene ontology (GO) enrichment analysis of biological processes inhibited by arsenic exposure in the WT mice. n = 5 mice per group.

[15,16] and (2) we found that arsenic induces NRF2 activation via the non-canonical p62-dependent mechanism [7]. Using arsenic treated WT, *Nrf2*$^{-/-}$, *p62*$^{-/-}$, and *Nrf2*$^{-/-}$;*p62*$^{-/-}$ mice, we demonstrate that p62-dependent non-canonical activation of NRF2 is essential for promoting insulin resistance and glucose intolerance in a chronic model of diabetes. Furthermore, detailed transcriptomic and metabolomic analyses reveal that prolonged NRF2 activation regulates liver fructose metabolism and gluconeogenesis, which could represent a key driver of changes in systemic blood glucose. Thus, our findings indicate a pro-diabetogenic role of non-canonical activation of the NRF2 pathway.

2. RESULTS

2.1. A non-canonical NRF2 model of diabetogenesis

To determine the pro-diabetogenic effects of p62-dependent non-canonical NRF2 activation, a chronic arsenic exposure model was used. Specifically, wild-type (WT), *Nrf2*$^{-/-}$, *p62*$^{-/-}$, and *Nrf2*$^{-/-}$;*p62*$^{-/-}$ mice were exposed to 0 or 25 ppm sodium arsenite in their drinking water for 20 weeks (Figure 1A). The arsenic-exposed WT mice did not exhibit any obvious change in total body mass, although the *p62*$^{-/-}$ and *Nrf2*$^{-/-}$;*p62*$^{-/-}$ mice weighed ~5 g more than the WT and *Nrf2*$^{-/-}$ mice at 20 weeks of age, consistent with the reported observation of p62$^{-/-}$

mice being obese starting at three months of age [17] (Figure 1B). Similarly, arsenic had no effect on liver weight or food intake but reduced water consumption in all of the mice genotypes (Figure S1A–C). Interestingly, arsenic exposure caused glucose intolerance and decreased insulin sensitivity in the WT but not $Nrf2^{-/-}$, $p62^{-/-}$, or $Nrf2^{-/-}$;$p62^{-/-}$ mice, whereas arsenic had no effects on serum insulin levels across all of the groups (Figure 1C—F), suggesting that loss of p62 and/or NRF2 counteracted arsenic-induced effects on insulin sensitivity and glucose tolerance.

2.2. Loss of NRF2 and/or p62 diminished arsenic-induced transcriptomic changes

To ascertain NRF2- and/or p62-dependent transcriptomic changes that might drive this pro-diabetic metabolic shift in the arsenic-treated WT mice, transcriptome sequencing was performed on liver tissues from all four of the mice genotypes. A heatmap of genes differentially regulated in the arsenic-exposed WT mice compared to the control WT mice indicated that transcriptomic changes induced by arsenic in a wild-type setting were lost in the $Nrf2^{-/-}$, $p62^{-/-}$, or $Nrf2^{-/-}$;$p62^{-/-}$ mice (Figure 2A). KEGG pathway enrichment using the upregulated portion of the geneset indicated that numerous aspects of amino acid, fatty acid, carbohydrate, lipid, and drug/xenobiotic metabolism were all significantly enhanced by arsenic (Figure 2B). Furthermore, hierarchical clustering and sign test analysis of genes differentially expressed across the different treatment and genotype combinations showed that the arsenic-exposed $Nrf2^{-/-}$ mice had a transcriptomic profile that most closely resembled that of the non-arsenic exposed WT controls, followed by the arsenic-exposed-$p62^{-/-}$ mice (Figure S2A–B). These data indicated that non-canonical NRF2 activation was a critical driver of the significant transcriptomic changes that occurred during arsenic exposure.

A more stringent in-depth analysis of the transcriptome sequencing results revealed that a total of 48 genes were significantly upregulated and 86 were downregulated in the livers of the arsenic-exposed WT mice compared to the controls (Supplementary Tables 1 and 2). Gene ontology (GO) enrichment analysis of the affected biological processes indicated that arsenic significantly upregulated genes involved in catabolic or reductive processes, including turnover of metabolic intermediates, oxidation/reduction reactions, and fatty acid/lipid metabolism, whereas genes involved in inflammation and the response to certain stressors/xenobiotics were downregulated (Figure 2C—D). Importantly, almost all of the observed arsenic-dependent gene expression changes in the WT mice were diminished in the arsenic-exposed $Nrf2^{-/-}$, $p62^{-/-}$, and $Nrf2^{-/-}$;$p62^{-/-}$ mice compared to their untreated controls (Figure 2C—D). Notably, 21 of the 48 genes upregulated by arsenic, including *Gclc*, *Gsta3*, *Gstm1*, *Abcc3*, *Ces1d*, and *Cyp2a5*, were established NRF2 target genes (Supplementary Table 1), none of which were upregulated in the arsenic-exposed $Nrf2^{-/-}$, $p62^{-/-}$, or $Nrf2^{-/-}$;$p62^{-/-}$ mice (Figure S3). These data, coupled with the known involvement of NRF2 in mediating the catabolic and xenobiotic stress response pathways during arsenic exposure, highlight the importance of non-canonical NRF2 activation in mediating this metabolic shift.

2.3. Arsenic-induced metabolic changes were p62-and/or NRF2-dependent

Based on the transcriptomic data indicating that the non-canonical activation of NRF2 promoted a shift in primary metabolic pathways, we next evaluated the global metabolome. Similar to the observed transcriptomic alterations, hierarchical clustering and sign test analyses revealed that the $Nrf2^{-/-}$ mice exposed to arsenic exhibited a metabolic profile similar to the WT control animals (Figure S4A–B). Furthermore,

loss of p62 and/or NRF2 shifted the subset of metabolites that were altered by arsenic exposure back to near the WT control levels, verifying an integral role of p62 and NRF2 in mediating the transcriptomic and subsequent metabolomic responses associated with pre-diabetic phenotypes (Figure 3A). As arsenic caused a modest but significant increase in fasting blood glucose levels, significant changes in key liver carbohydrate intermediates were assessed. Interestingly, the observed increase in carbohydrates that resulted from arsenic exposure in the WT mice was lost in the $Nrf2^{-/-}$, $p62^{-/-}$, or $Nrf2^{-/-}$;$p62^{-/-}$ arsenic-exposed mice (Figure 3B). Enrichment analysis of the carbohydrate-metabolizing pathways altered by arsenic revealed significant changes to the glycolysis, gluconeogenesis, pentose phosphate pathway, and fructose/mannose degradation (Figure 3C). These results, similar to the observed changes in the transcriptome, indicated that non-canonical NRF2 activation was essential for the metabolic reprogramming caused by prolonged arsenic exposure.

2.4. NRF2-dependent regulation of hepatic carbohydrate metabolism controlled glucose homeostasis

As both the transcriptomic and metabolomic data identified numerous metabolic pathways that were clearly affected by arsenic exposure, the next step was to determine which pathways were enriched in both datasets to ascertain the metabolic cascade most affected by non-canonical activation of NRF2. Consistent with the pathogenesis of diabetes, we observed an enrichment of four pathways only in the arsenic-treated WT mice: choline metabolism, fructose metabolism, valine/leucine/isoleucine degradation, and bile acid metabolism (Figure 4A). Since all of these pathways have been linked to liver glucose homeostasis, the transcriptional control of these pathways by NRF2 was investigated. Interestingly, WT but not $Nrf2^{-/-}$ liver slices treated with arsenic resulted in increased mRNA levels of the key fructose metabolism pathway enzymes ketohexokinase (*Khk*), sorbitol dehydrogenase (*Sord*), and triokinase/FMN cyclase (*Tkfc*) as well as a key mediator of liver gluconeogenesis hepatocyte nuclear factor 4 (*Hnf4A*) (Figure 4B). Intriguingly, assessment of other key gluconeogenic genes revealed that only *Hnf4A* was altered by arsenic in an NRF2-dependent manner, as glucose-6-phosphatase catalytic subunit 1 (*G6pc*) and phosphoenolpyruvate carboxykinase 1 (*Pck1*) levels increased, whereas forkhead box O1 (*Foxo1*) and PPARG coactivator 1 alpha (*Ppargc1a*) expression was unchanged in the WT and $Nrf2^{-/-}$ liver slices (Figure S5). An in silico analysis revealed a number of putative AREs in the promoter regions of *Khk*, *Sord*, *Tkfc*, and *Hnf4a*; thus, ChIP-PCR was performed on liver slices. Interestingly, NRF2-ARE binding was confirmed in all four targets, revealing fructose metabolism and gluconeogenesis as previously undiscovered branches of NRF2 regulation (Figure 4C). These data were confirmed in the arsenic-exposed WT mice, with liver tissue from these mice showing significant elevations in the transcript levels of these four enzymes that were reduced in the $Nrf2^{-/-}$ mice exposed to arsenic (Figure 4D). The notion that altered liver fructose metabolism and gluconeogenesis are major drivers of arsenic impairment of glucose homeostasis was further validated in an ex vivo liver tissue model using stable isotope labeling. Tissues were cultured in ^{13}C-fructose and the formation of ^{13}C-glucose and ^{13}C-sorbitol was quantified in each cohort. As shown in Figure 4E, ^{13}C-glucose was elevated in the media of the WT but not $Nrf2^{-/-}$ or $p62^{-/-}$ arsenic-exposed liver slices. Furthermore, the majority of fructose was metabolized into glucose and released but not converted into sorbitol via the polyol pathway, as the level of ^{13}C-sorbitol in the media was very low (less than 1% of the amount of ^{13}C-glucose) and was similar in untreated or arsenic-treated liver tissues (Figure 4E). Taken together, these results suggested that non-canonical activation of NRF2 by arsenic enhanced glucose production and release
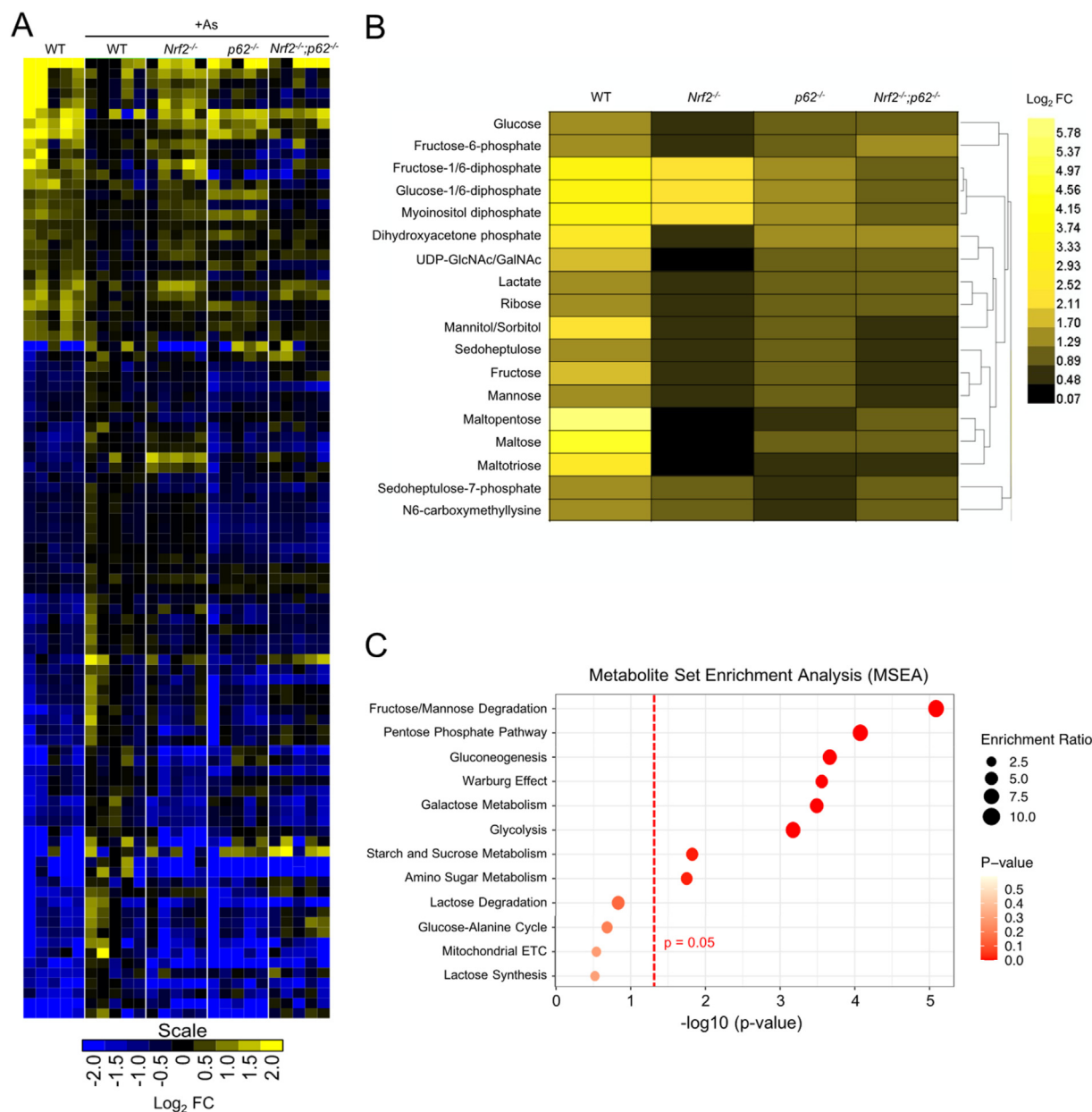
Figure 3: Arsenic-induced metabolic changes were p62-and/or NRF2-dependent. (A) Heatmap indicating log2 fold change of significantly altered metabolites across the indicated genotypes compared to controls. (B) Heatmap indicating carbohydrates were significantly increased by arsenic in a p62-and NRF2-dependent manner. n = 5 mice per group. (C) Pathway enrichment analysis of carbohydrate-metabolizing pathways significantly affected by arsenic exposure. Sizes of dots correspond to the enrichment ratio, which was computed by observed hits/expected hits using the MetaboAnalyst metabolite set enrichment analysis. Dot color indicates p value.

from the liver into the bloodstream via hepatic upregulation of key regulators of fructose metabolism and gluconeogenesis (Figure 4F).

3. DISCUSSION

The increased prevalence of type II diabetes continues to represent a global health crisis. It is estimated that ∼10% of the world's population aged 20−79 will be diabetic by 2030, resulting in over 4 million deaths and an absolute economic cost upward of 2 trillion U.S. dollars [18]. As the risk of developing type II diabetes continues to increase, so does the need to understand the basic molecular and cellular processes that drive pathogenesis. Importantly, diabetes does not represent a "one size fits all" disease, as a myriad of possible

underlying mechanisms have been proposed in a variety of contexts. However, a common unifying thread is a shift from normal homeostatic metabolism to a pro-pathogenic metabolic state. Herein, we show for the first time a "dark side" role of NRF2 in type II diabetes: prolonged non-canonical activation of NRF2, a critical regulator of cellular redox and metabolic homeostasis, is a key driver of a pro-diabetic shift in hepatic glucose metabolism. This diabetogenic shift in carbohydrate metabolism is driven by an NRF2-dependent upregulation of liver fructose metabolism and gluconeogenesis, as four enzymes that regulate these metabolic pathways were identified as novel NRF2 target genes. This finding not only implies that non-canonical NRF2 activation promotes diabetic outcomes, but also highlights a previously unknown facet of NRF2-regulated metabolism: increased hepatic
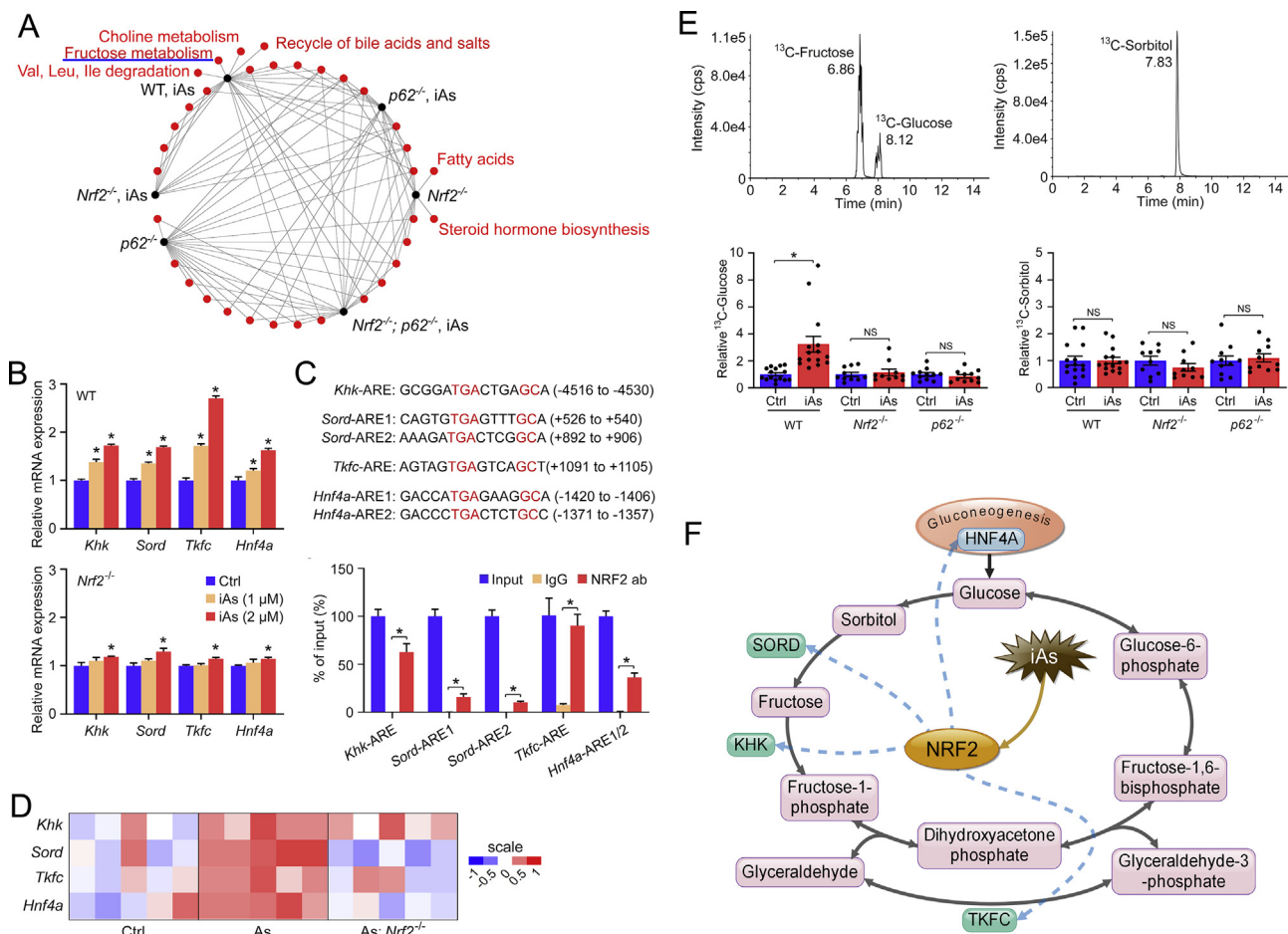
Figure 4: NRF2-dependent regulation of hepatic carbohydrate metabolism controlled glucose homeostasis. (A) Network diagram showing pathways enriched across different genotypes/treatment groups. Each black dot represents an indicated genotype/treatment group. Each red dot represents an enriched pathway. Pathways enriched in a particular genotype/treatment group are indicated by a line joining the red dots to the black dots. Pathway names are shown for those enriched in only one genotype/treatment group. (B) Relative mRNA levels of *Khk*, *Sord*, *Tkfc*, and *Hnf4A* from WT and *Nrf2*$^{-/-}$ liver slices cultured in normal media or media containing 1 or 2 μm of sodium arsenite for 16 h. (C) Putative ARE sequences and verification of NRF2-ARE binding via ChIP-PCR analysis. (D) RNAseq analysis of *Khk*, *Sord*, *Tkfc*, and *Hnf4A* transcript levels from the WT and *Nrf2*$^{-/-}$ mice exposed to 25 ppm of arsenic in the drinking water for 20 weeks. (E) LC-MS/MS analysis of ^{13}C-glucose and ^{13}C-sorbitol formation in WT, *Nrf2*$^{-/-}$, or *p62*$^{-/-}$ liver slices incubated in glucose-free medium containing ^{13}C-fructose for 16 h. The relative amount of ^{13}C-glucose or ^{13}C-sorbitol in the medium normalized to the total tissue protein levels are shown. (F) Schematic illustration of how NRF2 regulates fructose metabolism and gluconeogenesis following arsenic exposure.

glucose flux through the fructose metabolic and gluconeogenic cascades. Thus, a critical conclusion of this study is that non-canonical p62-dependent activation of NRF2 could be a key underlying cause of decreased insulin sensitivity and glucose intolerance observed in most diabetic patients, which represents a significant step forward in developing preventive/therapeutic strategies for type II diabetes.

4. MATERIALS AND METHODS

4.1. Animal experiments
All of the mice were handled according to the Guide for the Care and Use of Laboratory Animals, and all of the protocols were approved by the University of Arizona Institutional Animal Care and Use Committee. The generation of *Nrf2*$^{-/-}$ and *p62*$^{-/-}$ mice was reported previously [19,20]. In this study, four genotypes of mice were used, *Nrf2*$^{+/+}$;*p62*$^{+/+}$ (WT), *Nrf2*$^{-/-}$;*p62*$^{+/+}$ (Nrf2$^{-/-}$), *Nrf2*$^{+/+}$;*p62*$^{-/-}$ (p62$^{-/-}$), and *Nrf2*$^{-/-}$;*p62*$^{-/-}$ mice, which were generated by breeding *Nrf2*$^{+/-}$;*p62*$^{+/-}$ mice in a C57BL/6J background. For chronic arsenic exposure, 8- to 10-week-old mice (25—27 g) were randomly allocated

to the control (Ctrl) group or sodium arsenite (iAs) group (n = 5 mice per group). The mice in the Ctrl group received normal drinking water, while the mice in the iAs group received drinking water containing sodium arsenite (25 ppm) for 20 weeks. The amount of sodium arsenite (25 ppm) was chosen as it reflects the amount commonly used in the literature to obtain diabetic phenotypes [21,22]. Following exposure, water intake, food intake, and urine amounts were measured using specialty metabolic cages (PLEXX).

4.2. Intraperitoneal glucose tolerance test (GTT) and insulin tolerance test (ITT)
Following 20 weeks of iAs exposure, the mice from each group were fasted for 16 h. Glucose (2 g/kg, Sigma) and insulin (0.6 U/kg, Sigma) were administrated intraperitoneally for the GTT and ITT, respectively. A small volume of blood was removed from the tail vein, and blood glucose measurements were taken at time 0, followed by 15, 30, 60, 90, and 120 min post-injection using a OneTouch Blood Glucose Monitoring System (LifeScan). In addition, serum insulin levels were measured using a Mouse Insulin ELISA Kit (Thermo Fisher Scientific).

4.3. RNAseq analysis

To assess transcriptomic changes following iAs exposure, liver tissue from the 20-week-old Ctrl and iAs-treated WT, *Nrf2*$^{-/-}$, *p62*$^{-/-}$, and *Nrf2*$^{-/-}$;*p62*$^{-/-}$ mice was collected and snap frozen in liquid nitrogen (n = 5 mice per group X 8 groups = 40 samples). The samples were then sent to Qiagen Genomic Services (Qiagen) for subsequent RNA isolation, quantification, and quality control checks as well as cDNA preparation. Next-generation sequencing was then performed by Qiagen using a Qiagen UPX 3' Transcriptome Kit and an Illumina sequencing platform. Transcriptome sequencing data analyses were performed using the DESeq2 package to identify differentially expressed genes among the different genotype/treatment groups from count per gene data [23]. To determine the most significant changes, a false-discovery rate (FDR) of 0.05 was used as a statistical cut-off. A gene ontology analysis for enriched biological processes was then performed using the ShinyGo v0.61 web platform [24]. A sign test for consistency between two genesets was performed using a binomial test.

4.4. Metabolomics

Similar to the transcriptomic analysis, liver tissue from the 20-week-old Ctrl and iAs-treated WT, *Nrf2*$^{-/-}$, *p62*$^{-/-}$, and *Nrf2*$^{-/-}$;*p62*$^{-/-}$ mice was collected and snap frozen in liquid nitrogen (n = 5 mice per group X 8 groups = 40 samples). Samples were then sent to Metabolon for metabolomic analysis. Briefly, samples were prepared using the MicroLab STAR system (Hamilton). Proteins were removed via methanol precipitation and centrifugation, and the final extract was processed and analyzed using ultrahigh performance liquid chromatography-tandem mass spectroscopy (UPLC-MS/MS). Following the analysis, raw data were extracted and peaks were identified and validated by Metabolon. Metabolomic analyses were performed on Scaled Input Data provided by Metabolon. The data were first multiplied by a factor of 10,000 and then log2 transformed $[f(x) = log_2(x \times 10000)]$ to achieve homoscedasticity. The transformed data were analyzed using the Linear Model for Microarray Analysis (LIMMA) package to identify differentially enriched metabolites [25]. A metabolite set enrichment analysis (MSEA) was performed using the MetaboAnalyst 4.0 web platform [26]. A sign test for consistency between two metabolite sets was performed using a binomial test.

4.5. Combined dataset pathway enrichment analysis

Combined transcriptomic and metabolomic analysis was performed by first assigning each gene and metabolite to their respective Bio-Systems ID (NCBI BioSystems Database). Pathway enrichment for gene expression was determined using a hypergeometric test, and the resulting p values were corrected for multiple testing according to the method described by Benjamini and Hochberg [27]. This correction is based on the assumption that transcriptional reprogramming changes by differential activation of specific transcription factors, leading to coordinated over- and/or under-expression of a particular set of genes. Pathway enrichment for differentially enriched metabolites is solely based on annotation alone. This is based on the assumption that when metabolic reprogramming occurs, the metabolic pathway involved will enter a constant flux, resulting in only a few metabolites within the pathway showing a significant change in concentration. The enriched pathway BioSystems IDs from the gene expression analysis were then intersected with those from the metabolite analyses to identify pathways altered in each comparison pair.

4.6. Real-time qRT-PCR (qPCR) analysis

Fresh liver tissue was isolated from the WT or *Nrf2*$^{-/-}$ mice and cut into 150 μm thick sections using a vibratome tissue slicer (Precisionary

Instruments). The tissue slices were then left untreated or treated with iAs (1 μM or 2 μM) for 16 h. Following treatment, total mRNA was extracted using TRIzol (Invitrogen) according to the manufacturer's instructions. The cDNA was synthesized using 2 μg of RNA and a Transcriptor First-Strand cDNA Synthesis Kit (Promega). Mouse *Actb* levels were used for qPCR normalization, and all of the experiments were performed in triplicate. The primer sequences were as follows:

Khk-F-ATGTGGTGGACAAATACCCAGA
Khk-R-CAAGCAAGGAAAGGACAGTGC
Sord-F-GCTAAGGGCGAGAACCTGTC
Sord-R-CATGCTCCCAGTAGTGAACATC
Tkfc-F-CCTTGCTGGGTTAGTAGCCTC
Tkfc-R-CTTTCCCGATAAAACCGGCAT
Hnf4a-F-CACGCGGAGGTCAAGCTAC
Hnf4a-R-CCCAGAGATGGGAGAGGTGAT
Actb-F-AAGGCCAACCGTGAAAAGAT
Actb-R-GTGGTACGACCAGAGGCATAC

4.7. Chromatin immunoprecipitation (ChIP)-qPCR

A ChIP assay was performed according to the manufacturer's instructions (EZ-CHIPTM, Merck, Germany). Briefly, 150 μm thick liver sections were treated with 1% formaldehyde in DMEM for 10 min to cross-link DNA-protein complexes. The tissue sections then were lysed using SDS lysis buffer containing 1 mM of phenylmethylsulfonyl fluoride (PMSF) and 1% protease inhibitor cocktail (Sigma). Solubilized chromatin was then incubated with anti-NRF2 antibody (Santa Cruz Biotechnology) or normal rabbit IgG (Santa Cruz Biotechnology) for 16 h at 4 °C with rotation, and DNA-protein complexes were pulled down using Protein G-agarose beads (Sigma). DNA from the immunoprecipitated complexes and total chromatin input were extracted via ethanol precipitation, and 1 μL of purified DNA was used for qPCR detection. The primer sequences were as follows:

Khk-ARE-F-AGTTGGAGTAGGCAGAGACTG
Khk-ARE-R-TTTGGTCAGACTCTTCACCTG
Sord-ARE1-F-AAACTAATCAAGCCTTCGACTC
Sord-ARE1-R-TAAATGCCACCATGCCACCT
Sord-ARE2-F-TACCTCTGCCTCTGGCTTTA
Sord-ARE2-R-GAGATGGCTGGTATCCAATC
Tkfc-ARE-F-CAAGTCCTAACTCTCAGCAAC
Tkfc-ARE-R-GAATCATGTCCAGCTTAAAGC
Hnf4a-ARE1/2-F-GAAAGCAAGTGAACTGAGGAGC
Hnf4a-ARE1/2-R-CAGCTACTCTCTCTCAGTCTCT

4.8. Analysis of ^{13}C-glucose, ^{13}C-sorbitol, and ^{13}C-fructose by LC-MS/MS

The levels of ^{13}C-glucose and ^{13}C-sorbitol formed and ^{13}C-fructose remaining in the culture media were measured. Approximately 20 μL of the culture media was moved to glass tubes containing 10 μL of internal standard (methyl α-D-glucopyranoside in water). After vortexing for 15 s, 300 μL of ice-cold acetonitrile were added to the samples, vortexed for 1 min, and centrifuged at 3700 rpm for 15 min to precipitate protein. The supernatant was transferred to a clean glass tube and dried at room temperature under nitrogen. The residue was dissolved with 500 μL of water and extracted by solid phase extraction. Isolute multimode mixed-mode solid-phase extraction columns (Biotage, Charlotte, NC, USA) were used. The columns were conditioned with 1 mL of acetonitrile and then equilibrated with 1 mL of water. The water-dissolved residues were loaded onto the columns, which were then washed with 500 μL of water. The flow-through was collected and combined equaling a volume of approximately 1 mL. After centrifuging at 3700 rpm for 15 min, an equal volume of acetonitrile

was added to each supernatant and the samples were subjected to LC-MS/MS for analysis. The amount of ^{13}C-fructose obtained from the liver slice-free controls was compared to the amount of ^{13}C-glucose or ^{13}C-sorbitol and expressed as the percentage of the liver slice-free control per mg of protein (%/mg protein), respectively.

4.9. LC—MS/MS analyses

^{13}C-glucose, ^{13}C-sorbitol, and ^{13}C-fructose were analyzed on an AB-SCIEX model Q-Trap 6500 mass spectrometer (AB-SCIEX, Framingham, MA, USA) interfaced online with a 1290 Infinity Series ultra-performance liquid chromatography system. Chromatographic separation was carried out with an ACQUITY UPLC BEN Amide column (1.7 μm and 2.1 × 150 mm; Waters) by gradient elution at a flow rate of 0.3 mL/min for 15 min. The mobile phases were composed of 0.025% (v/v) ammonium hydroxide in water (A) and 0.025% (v/v) ammonium hydroxide in acetonitrile (B). The linear gradient was as follows: 10—26% A for 0—8.5 min, 26-10% A for 8.5—9 min, and 10% A for 9—15 min ^{13}C-glucose, ^{13}C-sorbitol, and ^{13}C-fructose were analyzed in the negative ion mode by multiple reaction monitoring scanning. The transitions were m/z 185.2/91.9 for ^{13}C-glucose and ^{13}C-fructose, m/z 187.1/92.0 for ^{13}C-sorbitol, and m/z 193.2/100.9 for the internal standard. All of the data were analyzed using AB SCIEX Analyst 1.6.3 software (Applied Biosystems).

4.10. Computational and statistical analyses

All of the results are presented as mean ± SD, and a biological statistical analysis was performed using GraphPad Prism 8. Student's t tests were used to compare the means of two groups, and one-way ANOVA with Bonferroni's correction was used to compare the means of three or more groups. $p < 0.05$ was considered statistically significant. All of the computational statistical analyses were performed in the R statistical environment.

AUTHOR CONTRIBUTIONS

P.L., M.D., A.O., and D.Z. conceptualized the study. P.L., M.D., H.L., C.J.S., A.S., and Y.W. generated, analyzed, and arranged the data included in the figures and tables. M.D., P.L., A.O., and D.D.Z. wrote the manuscript. E.C., P.R.K., Q.Z., X.D., J.G.N.G., and E.W. edited the manuscript and provided feedback. A.O. and D.D.Z. supervised the study. A.O. performed the biostatistical analysis.

ACKNOWLEDGMENTS

CONFLICT OF INTEREST

None declared.

APPENDIX A. SUPPLEMENTARY FIGURE
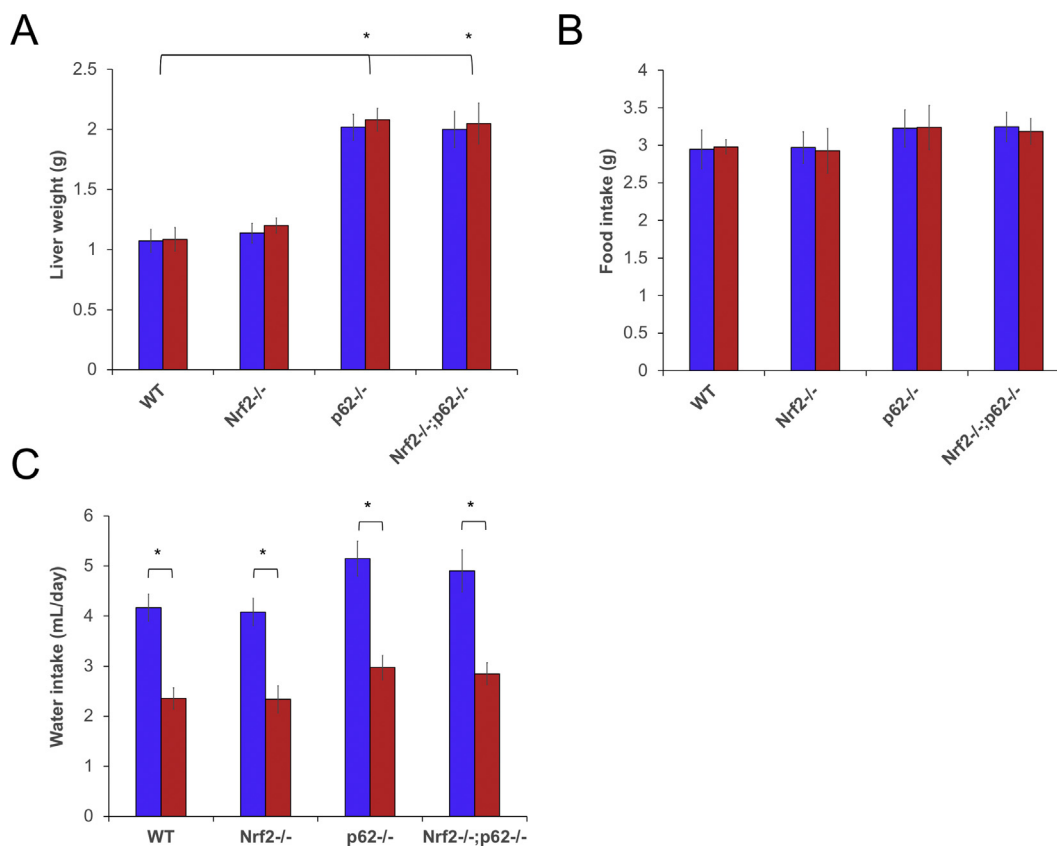
Figure S1: Arsenic does not alter liver weight, food intake, or water intake. (A) Liver weight, (B) Food intake, and (C) Water intake in 20-week WT, $Nrf2^{-/-}$, $p62^{-/-}$, and $Nrf2^{-/-};p62^{-/-}$ arsenic treated mice compared to control.
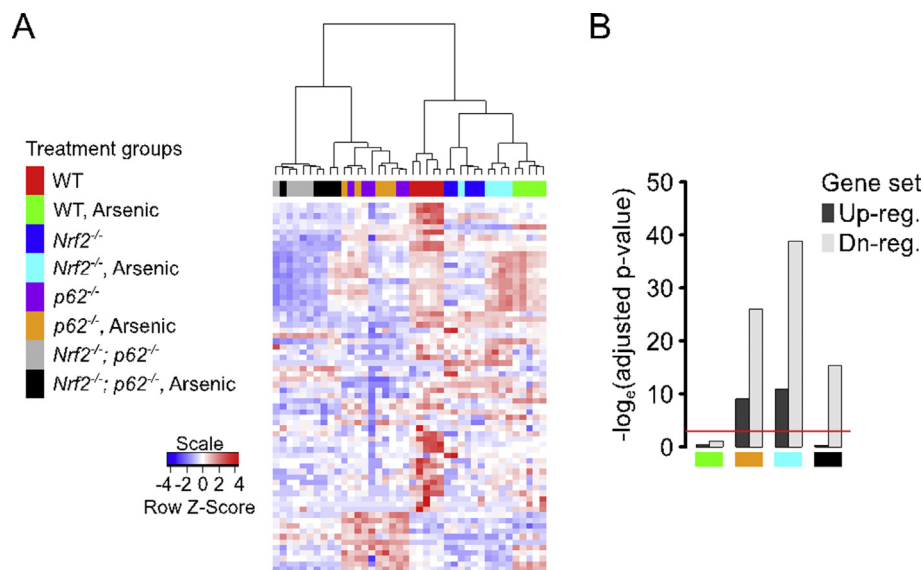
Figure S2: Loss of NRF2 and/or p62 diminishes arsenic-induced transcriptomic variability. (A) Hierarchical clustering analysis and (B) Geneset test of transcriptomic changes in 20-week WT, $Nrf2^{-/-}$, $p62^{-/-}$, and $Nrf2^{-/-};p62^{-/-}$ arsenic treated mice compared to WT untreated control. Red line represents p = 0.05.
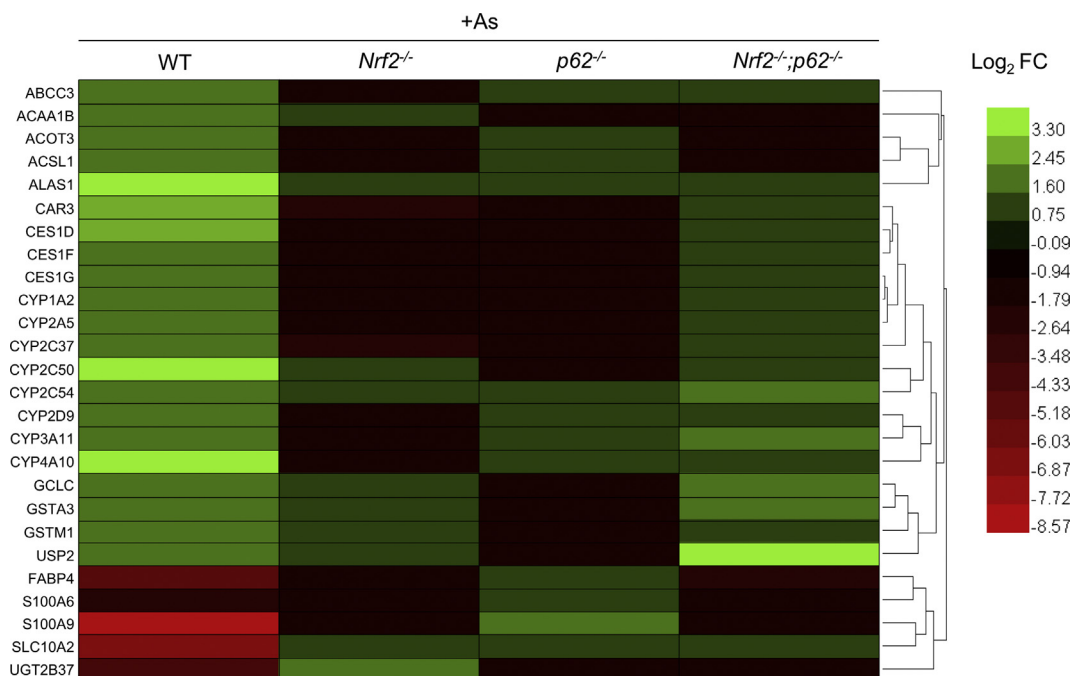
Figure S3: NRF2 target genes altered by arsenic exposure. Heatmap indicating transcripts identified by RNAseq to significantly increase or decrease following arsenic exposure in WT, but not $Nrf2^{-/-}$, $p62^{-/-}$, or $Nrf2^{-/-};p62^{-/-}$ arsenic-exposed mice. n = 5 mice per group.
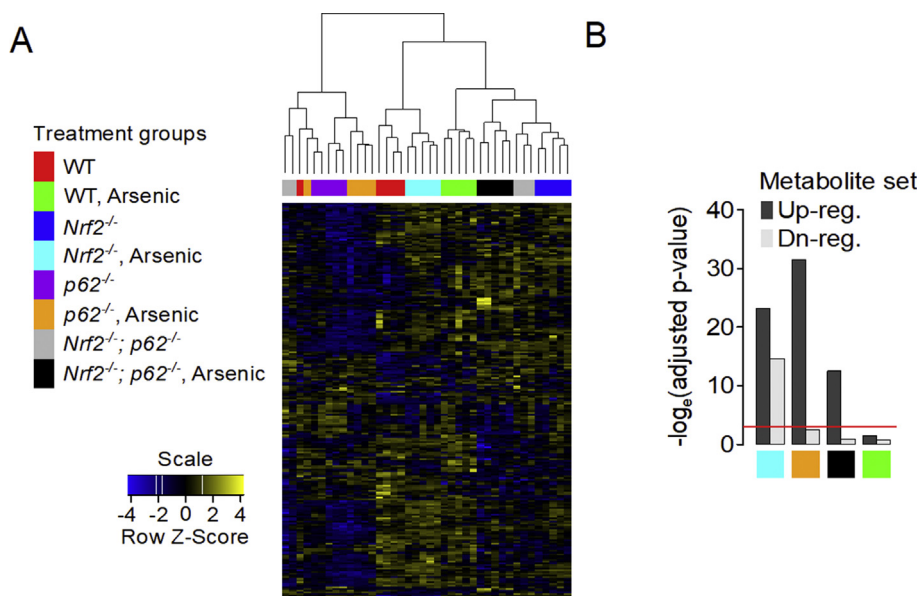
Figure S4: Loss of NRF2 and/or p62 diminishes arsenic-induced metabolomic variability. (A) Hierarchical clustering analysis and (B) Geneset test of metabolomic changes in 20-week WT, *Nrf2*^{−/−}, *p62*^{−/−}, and *Nrf2*^{−/−};*p62*^{−/−} arsenic treated mice compared to WT untreated control. Red line represents p = 0.05.
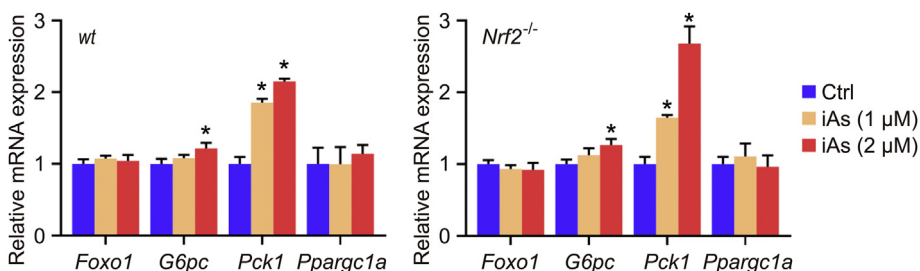
Figure S5: Arsenic causes an NRF2-independent increase in other gluconeogenic genes. Relative mRNA levels of *Foxo1*, *G6pc*, *Pck1*, and *Ppargc1a* from WT and *Nrf2*^{−/−} liver slices cultured in normal media, or media containing 1 or 2 μm sodium arsenite for 16 h.

Supplemental Table 1 — Genes significantly upregulated by Arsenic exposure

Category	Gene	Function	NRF2[Ref]	FC
Amino acid metabolism	*Afmid*	Tryptophan degradation		2.448
	Pah	L-tyrosine formation		1.826
	Sardh	Oxidative demethylation of sarcosine		1.956
	Uroc1	Formiminoglutamic acid formation in histidine catabolism		1.987
DNA synthesis/repair	*Tk1*	dTMP formation		4.524
	Upp2	Uridine and deoxyuridine cleavage to uracil and ribose-/deoxyribose-1-phosphate		2.288
	Usp2	MDM2, MDM4, and CCND1 deubiquitylation	[28]	3.570
Drug/Xenobiotic metabolism	*Abca8a*	Molecular transport across internal and external membranes		2.564
	Abcc3	MTX and 7OH-MTX transport from liver into circulation	[29]	2.124
	Cyp1a2	Carbon-hydrogen bonds hydroxylation	[30]	1.964
	Cyp2a5	Coumarin 7-hydroxylase activity	[31]	3.827
	Cyp2c37	Arachidonic acid metabolism	[32]	2.046
	Cyp2c50	Arachidonic acid metabolism	[33]	2.045
	Cyp2c54	Arachidonic acid metabolism	[34]	2.101
	Cyp2d9	Steroid, fatty acid, and xenobiotic oxidation	[35]	2.338
	Cyp3a11	Erythromycin N-demethylation, nifedipine oxidation and testosterone 6 beta-hydroxylation	[36]	2.164
	Cyp3a25	Steroid, fatty acid, and xenobiotic oxidation		1.909
	Cyp4a10	Steroid, fatty acid, and xenobiotic oxidation	[37]	1.892
	Inmt	N-methylation of indoles		2.966

Supplemental Table 1 — *(continued)*

Category	Gene	Function	NRF2Ref	FC
	Rdh16	9-cis-retinoic acid biosynthesis		2.266
	Ugt2a3	Conjugation of lipophilic substrates with glucuronic acid to enhance excretion		2.282
Fatty acid metabolism	Acaa1b	Fatty acid beta-oxidation and phenylacetate catabolism	[38]	1.889
	Acot3	Acyl-CoA hydrolysis	[39]	3.138
	Acsl1	Long-chain fatty acid conversion	[40]	1.796
	Apol9b	Lipid binding		2.453
	Ces1d	Triacylglycerol and monoacylglycerol hydrolysis	[34]	4.144
	Ces1e	Retinyl ester hydrolysis.		2.519
	Ces1f	Triacylglycerol and monoacylglycerol hydrolysis	[41]	2.019
	Ces1g	Ester, thioester, or amide bond hydrolysis	[42]	2.936
	Etnppl	Phosphoethanolamine breakdown		3.279
Detoxification (GSH-based system)	Gclc	Glutathione synthesis	[43]	1.851
	Gsta3	Glutathione conjugation to electrophiles	[44]	2.167
	Gstm1	Glutathione conjugation to electrophiles	[44]	2.006
Heme biosynthesis	Alas1	Synthesis of 5-aminolevulinate from glycine	[45]	1.953
	Klkb1	Cleaves Lys—Arg and Arg—Ser bonds and is involved in blood coagulation		1.700
Hormone metabolism	Hsd17b6	Oxidoreductase and epimerase involved in androgen catabolism		2.201
	Hsd3b3	Enzyme involved in oxidative conversion of ketosteroids; involved in biosynthesis of hormonal steroids		2.075
	Serpina6	Transport protein for glucorticoids and progestins		2.401
	Slco1a4	Mediates transport of hormones		2.504
Miscellaneous	Mup-ps19	Pseudo gene		2.065
	Tsku	Intracellular transport and extracellular secretion		3.143
Muscle/Bone structure/function	Car3	Carbon dioxide hydration	[46]	2.282
	Fam210a	Bone structure and function regulation		2.147
Carbohydrate metabolism	Dbp	Transcriptional activator		2.548
	Dcxr	Diacetyl reductase and L-xylulose reductase that may play a role in glucose metabolism via uronate cycle		2.276
	Gys2	Glycogen synthesis		1.918
	Hyi	Hydroxypyruvate to 2-hydroxy-3-oxopropanoate conversion		2.646
	Pdxk	Vitamin B6 phosphorylation		2.729

Supplemental Table 2 — Genes significantly downregulated by Arsenic exposure

Category	Gene	Function	NRF2Ref	FC
DNA function/repair	Apcs	Serum form of amyloid P component		−7.888
	Rad51b	Interacts with RAD51 family proteins in homologous recombination		−2.587
Fatty acid metabolism	Fabp4	Fatty acid binding protein involved in long-chain fatty acid and retinoic acid delivery	[47]	−4.809
	Ldha	Subunit of lactate dehydrogenase involved in pyruvate conversion to lactate		−1.786
Heme biosynthesis	Cpb2	Fibrinolysis downregulation catalyzed by fibrin C-terminal residue removal		−1.99
	Fga	Alpha subunit of coagulation factor fibrinogen		−2.969
	Fgb	Beta subunit of coagulation factor fibrinogen		−2.828
	Fgg	Gamma subunit of coagulation factor fibrinogen		−3.173
	Fgl1	Homologous to Fgb and Fgg but lacks sites necessary for clot formation		−3.740
	Hp	Haptoglobin formation		−2.752
	Hpx	High affinity heme binding		−2.938
	Serpina10	Coagulation factor inhibition		−2.669
Hormone metabolism	Igfbp1	Binds to insulin-like growth factors extending their half life		−5.147
	Serpina7	Binds and transports thyroid hormones in circulation		−2.795
Immune response	Cd24a	Sialoglycoprotein and cell adhesion molecule expressed in B lymphocytes and neuroblasts		−4.666
	Cfh	Complement regulation of immune response		−2.285
	Ctsc	Serine proteinase activation in immune cells		−1.875
	Lbp	Binds to bacterial lipopolysaccharide to elicit immune response		−2.120
	Ly6d	B-cell specification marker		−4.458

Supplemental Table 2 — *(continued)*

Category	Gene	Description	Ref	Value
Inflammatory response	Cxcl1	Chemokine that signals through CXCR2		−9.397
	Il13ra1	Subunit of interleukin receptor important in fibrosis		−2.641
	Il1r1	Subunit of cytokine receptor important in inflammation		−2.194
	Itih4	Cleaved by plasma kallikrein and related to inflammatory response		−2.395
	Orm1	Acute-phase reactant		−4.236
	Orm2	Acute-phase reactant		−11.201
	Saa1	Acute-phase reactant		−11.664
	Saa2	Acute-phase reactant		−13.269
	Saa3	Acute-phase reactant		−10.595
	Socs3	Binds to tyrosine kinase receptors to inhibit cytokine signaling		−5.186
	Socs5	Unknown function but contains SH2 and SOCS BOX domain		−4.832
Metal/xenobiotic metabolism	Mt1	Binds various metals via cysteine residues		−5.519
	Mt2	Binds various metals via cysteine residues		−7.940
	Nnmt	Methyl donation of S-adenosyl methionine		−2.457
	Steap4	Iron and copper metalloreductase		−2.841
	Ugt2b37	Glucuronosyltransferase activity important in conjugation and elimination of xenobiotics	[48]	−3.875
Miscellaneous	Apoa4	Unknown function but involved in cholesterol metabolism		−2.122
	Cyp2c70	Hydroxylates major bile acids at 6-beta position. Involved in muricholic acid synthesis		−2.231
	Fam102b	Unknown function		−6.299
	Fam25c	Unknown function		−2.861
	Prkca	Serine—threonine protein kinase of various targets		−2.123
	Sdf2l1	Unknown function but interacts with ER-associated degradation machinery		−2.789
	Snhg18	RNA gene affiliated with lncRNA		−7.211
Muscle/Bone structure/function	Car2	Carbon dioxide hydration		−3.087
Nervous system	Chrm3	Muscarinic cholinergic receptor that binds acetylcholine		−3.146
	Grid2	Excitatory neurotransmitter receptor		−5.680
	Pld1	Catalyzes phosphatidylcholine hydrolysis		−4.475
	Smpd3	Catalyzes sphingomyelin hydrolysis		−7.122
Proliferation and differentiation	Cdkn1a	Binds to and inhibits cyclin/CDK complexes		−3.047
	Egr1	Transcriptional regulator that binds to DNA and is important for differentiation and mitogenesis		−9.069
	Fndc3b	Adipocyte differentiation		−2.468
	Gas6	Cell proliferation		−3.567
	Hbegf	Growth factor that promotes smooth muscle cell proliferation		−6.289
	Reg2	Related to pancreatic beta cell proliferation		−96.535
	S100a6	Cell cycle progression and differentiation	[49]	−8.569
	S100a9	Cell cycle progression and differentiation	[50]	−6.725
	Serpina3n	Member of serine protease inhibitor class that may be involved in vascularization		−4.804
	Tacc2	Microtubule-dependent coupling of the nucleus and centrosome		−2.767
Signal transduction and transcriptional regulators	Camk2d	Calcium-dependent protein kinase involved in calcium homeostasis		−2.339
	Dmbt1	Poly-sulfated/phosphorylated ligand binding		−5.667
	Glis3	Transcriptional regulator		−4.138
	Gnat1	Rhodopsin and CGMP-phoshodiesterase coupling		−4.200
	Hnf4g	Transcription factor associated with cell proliferation		−14.023
	Junb	Transcription factor known for tumor suppressor activity		−2.576
	Litaf	DNA-binding protein that regulates TNF-alpha expression		−1.982
	Lrg1	Involved in protein—protein interactions (i.e. endoglin)		−2.492
Structural components	Cfap69	Flagella assembly		−13.790
	Cldn2	Integral tight junction protein		−2.090
	Crybb3	Dominant structural component of eye		−7.335
	Itih3	Extracellular matrix stabilization		−1.886
	Krt19	Structural integrity of epithelial cells		−7.501
	Lamb1	Basement membrane constituent		−3.439
	Mid1	Association with microtubules for multiprotein structure		−3.908
	Neat1	Core structural lncRNA		−2.293
	Prg4	Proteoglycan synthesized by chondrocytes		−2.650
	Prtn3	Collagen degradation		−11.060

Supplemental Table 2 — *(continued)*

Sugar metabolism	*B3galt1*	Transfers galactose from UDP-alpha-ᴅ-galactose to various substrates		−2.532
	Fut8	Catalyzes transfer of fucose from GDP-fucose to reducing terminal GlcNAc of Asn-linked oligosaccharide		−3.640
Transport proteins and channels	*Ano1*	Chloride and bicarbonate channeling		−4.968
	Crip1	Zinc transport		−3.966
	Lcn2	Hydrophobic molecule transport		−14.204
	Mvp	Vault complex formation for nucleo-cytoplasmic transport		−2.286
	S100g	Correlation with calcium transport activity		−10.970
	Scara5	Ferritin receptor		−4.475
	Slc10a2	Sodium/bile acid transport	[51]	−2.560
	Slc26a3	Chloride and bicarbonate transport		−40.317
	Slc3a1	Renal amino acid transport		−2.255

REFERENCES

[1] Dodson, M., de la Vega, M.R., Cholanians, A.B., Schmidlin, C.J., Chapman, E., Zhang, D.D., 2019. Modulating NRF2 in disease: timing is everything. Annual Review of Pharmacology and Toxicology 59:555–575.

[2] Rojo de la Vega, M., Chapman, E., Zhang, D.D., 2018. NRF2 and the hallmarks of cancer. Cancer Cell 34(1):21–43.

[3] Zhang, D.D., Lo, S.C., Cross, J.V., Templeton, D.J., Hannink, M., 2004. Keap1 is a redox-regulated substrate adaptor protein for a Cul3-dependent ubiquitin ligase complex. Molecular and Cellular Biology 24(24):10941–10953.

[4] Zhang, D.D., Hannink, M., 2003. Distinct cysteine residues in Keap1 are required for Keap1-dependent ubiquitination of Nrf2 and for stabilization of Nrf2 by chemopreventive agents and oxidative stress. Molecular and Cellular Biology 23(22):8137–8151.

[5] Sun, Z., Zhang, S., Chan, J.Y., Zhang, D.D., 2007. Keap1 controls post-induction repression of the Nrf2-mediated antioxidant response by escorting nuclear export of Nrf2. Molecular and Cellular Biology 27(18):6334–6349.

[6] Lau, A., Wang, X.J., Zhao, F., Villeneuve, N.F., Wu, T., Jiang, T., et al., 2010. A noncanonical mechanism of Nrf2 activation by autophagy deficiency: direct interaction between Keap1 and p62. Molecular and Cellular Biology 30(13): 3275–3285.

[7] Lau, A., Zheng, Y., Tao, S., Wang, H., Whitman, S.A., White, E., et al., 2013. Arsenic inhibits autophagic flux, activating the Nrf2-Keap1 pathway in a p62-dependent manner. Molecular and Cellular Biology 33(12):2436–2446.

[8] Dodson, M., Liu, P., Jiang, T., Ambrose, A.J., Luo, G., Rojo de la Vega, M., et al., 2018. Increased O-GlcNAcylation of SNAP29 drives arsenic-induced autophagic dysfunction. Molecular and Cellular Biology.

[9] Dodson, M., Zhang, D.D., 2017. Non-canonical activation of NRF2: new insights and its relevance to disease. Curr Pathobiol Rep 5(2):171–176.

[10] Ramos-Gomez, M., Kwak, M.K., Dolan, P.M., Itoh, K., Yamamoto, M., Talalay, P., et al., 2001. Sensitivity to carcinogenesis is increased and chemoprotective efficacy of enzyme inducers is lost in nrf2 transcription factor-deficient mice. Proc Natl Acad Sci U S A 98(6):3410–3415.

[11] Lau, A., Villeneuve, N.F., Sun, Z., Wong, P.K., Zhang, D.D., 2008. Dual roles of Nrf2 in cancer. Pharmacological Research 58(5–6):262–270.

[12] Hayes, J.D., Dinkova-Kostova, A.T., Tew, K.D., 2020. Oxidative stress in cancer. Cancer Cell 38(2):167–197.

[13] Roden, M., Shulman, G.I., 2019. The integrative biology of type 2 diabetes. Nature 576(7785):51–60.

[14] Ling, C., Ronn, T., 2019. Epigenetics in human obesity and type 2 diabetes. Cell Metabolism 29(5):1028–1044.

[15] Navas-Acien, A., Silbergeld, E.K., Pastor-Barriuso, R., Guallar, E., 2008. Arsenic exposure and prevalence of type 2 diabetes in US adults. Journal of the American Medical Association 300(7):814–822.

[16] Wang, W., Xie, Z., Lin, Y., Zhang, D., 2014. Association of inorganic arsenic exposure with type 2 diabetes mellitus: a meta-analysis. Journal of Epidemiology & Community Health 68(2):176–184.

[17] Rodriguez, A., Duran, A., Selloum, M., Champy, M.F., Diez-Guerra, F.J., Flores, J.M., et al., 2006. Mature-onset obesity and insulin resistance in mice deficient in the signaling adapter p62. Cell Metabolism 3(3):211–222.

[18] Bommer, C., Sagalova, V., Heesemann, E., Manne-Goehler, J., Atun, R., Barnighausen, T., et al., 2018. Global economic burden of diabetes in adults: projections from 2015 to 2030. Diabetes Care 41(5):963–970.

[19] Chan, K., Lu, R., Chang, J.C., Kan, Y.W., 1996. NRF2, a member of the NFE2 family of transcription factors, is not essential for murine erythropoiesis, growth, and development. Proc Natl Acad Sci U S A 93(24):13943–13948.

[20] Duran, A., Serrano, M., Leitges, M., Flores, J.M., Picard, S., Brown, J.P., et al., 2004. The atypical PKC-interacting protein p62 is an important mediator of RANK-activated osteoclastogenesis. Developmental Cell 6(2):303–309.

[21] Paul, D.S., Devesa, V., Hernandez-Zavala, A., Adair, B.M., Walton, F.S., Drobna, Z., et al., 2008. Environmental arsenic as a disruptor of insulin signaling. Met Ions Biol Med 10:1–7.

[22] Paul, D.S., Walton, F.S., Saunders, R.J., Styblo, M., 2011. Characterization of the impaired glucose homeostasis produced in C57BL/6 mice by chronic exposure to arsenic and high-fat diet. Environmental Health Perspectives 119(8):1104–1109.

[23] Love, M.I., Huber, W., Anders, S., 2014. Moderated estimation of fold change and dispersion for RNA-seq data with DESeq2. Genome Biology 15(12):550.

[24] Ge, S.X., Jung, D., Yao, R., 2020. ShinyGO: a graphical gene-set enrichment tool for animals and plants. Bioinformatics 36(8):2628–2629.

[25] Ritchie, M.E., Phipson, B., Wu, D., Hu, Y., Law, C.W., Shi, W., et al., 2015. Limma powers differential expression analyses for RNA-sequencing and microarray studies. Nucleic Acids Research 43(7):e47.

[26] Chong, J., Xia, J., 2020. Using MetaboAnalyst 4.0 for metabolomics data analysis, interpretation, and integration with other omics data. Methods in Molecular Biology 2104:337–360.

[27] Benjamini, Y., Hochberg, Y., 1995. Controlling the false discovery rate - a practical and powerful approach to multiple testing. Journal of the Royal Statistical Society - Series B: Statistical Methodology 57(1):289–300.

[28] Yates, M.S., Tran, Q.T., Dolan, P.M., Osburn, W.O., Shin, S., McCulloch, C.C., et al., 2009. Genetic versus chemoprotective activation of Nrf2 signaling: overlapping yet distinct gene expression profiles between Keap1 knockout and triterpenoid-treated mice. Carcinogenesis 30(6):1024–1031.

[29] Canet, M.J., Merrell, M.D., Harder, B.G., Maher, J.M., Wu, T., Lickteig, A.J., et al., 2015. Identification of a functional antioxidant response element within the eighth intron of the human ABCC3 gene. Drug Metabolism & Disposition 43(1):93–99.

[30] Walsh, J., Jenkins, R.E., Wong, M., Olayanju, A., Powell, H., Copple, I., et al., 2014. Identification and quantification of the basal and inducible Nrf2-dependent proteomes in mouse liver: biochemical, pharmacological and toxicological implications. J Proteomics 108:171—187.

[31] Abu-Bakar, A., Lamsa, V., Arpiainen, S., Moore, M.R., Lang, M.A., Hakkola, J., 2007. Regulation of CYP2A5 gene by the transcription factor nuclear factor (erythroid-derived 2)-like 2. Drug Metabolism & Disposition 35(5):787—794.

[32] Barve, A., Khor, T.O., Nair, S., Lin, W., Yu, S., Jain, M.R., et al., 2008. Pharmacogenomic profile of soy isoflavone concentrate in the prostate of Nrf2 deficient and wild-type mice. Journal of Pharmacological Sciences 97(10): 4528—4545.

[33] Chartoumpekis, D.V., Wakabayashi, N., Kensler, T.W., 2015. Keap1/Nrf2 pathway in the frontiers of cancer and non-cancer cell metabolism. Biochemical Society Transactions 43(4):639—644.

[34] Wu, K.C., Cui, J.Y., Klaassen, C.D., 2012. Effect of graded Nrf2 activation on phase-I and -II drug metabolizing enzymes and transporters in mouse liver. PloS One 7(7):e39006.

[35] Kwak, M.K., Wakabayashi, N., Itoh, K., Motohashi, H., Yamamoto, M., Kensler, T.W., 2003. Modulation of gene expression by cancer chemo-preventive dithiolethiones through the Keap1-Nrf2 pathway. Identification of novel gene clusters for cell survival. Journal of Biological Chemistry 278(10): 8135—8145.

[36] Shen, G., Kong, A.N., 2009. Nrf2 plays an important role in coordinated regulation of Phase II drug metabolism enzymes and Phase III drug transporters. Biopharmaceutics & Drug Disposition 30(7):345—355.

[37] Shen, G., Xu, C., Hu, R., Jain, M.R., Gopalkrishnan, A., Nair, S., et al., 2006. Modulation of nuclear factor E2-related factor 2-mediated gene expression in mice liver and small intestine by cancer chemopreventive agent curcumin. Molecular Cancer Therapeutics 5(1):39—51.

[38] Kitteringham, N.R., Abdullah, A., Walsh, J., Randle, L., Jenkins, R.E., Sison, R., et al., 2010. Proteomic analysis of Nrf2 deficient transgenic mice reveals cellular defence and lipid metabolism as primary Nrf2-dependent pathways in the liver. Journal of Proteomics 73(8):1612—1631.

[39] Paek, J., Lo, J.Y., Narasimhan, S.D., Nguyen, T.N., Glover-Cutter, K., Robida-Stubbs, S., et al., 2012. Mitochondrial SKN-1/Nrf mediates a conserved starvation response. Cell Metabolism 16(4):526—537.

[40] Chen, Y., He, L., Yang, Y., Chen, Y., Song, Y., Lu, X., et al., 2019. The inhibition of Nrf2 accelerates renal lipid deposition through suppressing the ACSL1 expression in obesity-related nephropathy. Renal Failure 41(1):821—831.

[41] Knatko, E.V., Tatham, M.H., Zhang, Y., Castro, C., Higgins, M., Dayalan Naidu, S., et al., 2020. Downregulation of Keap1 confers features of a fasted metabolic state. iScience 23(10):101638.

[42] Zhang, Y., Cheng, X., Aleksunes, L., Klaassen, C.D., 2012. Transcription factor-mediated regulation of carboxylesterase enzymes in livers of mice. Drug Metabolism & Disposition 40(6):1191—1197.

[43] Chan, K., Kan, Y.W., 1999. Nrf2 is essential for protection against acute pulmonary injury in mice. Proceedings of the National Academy of Sciences of the United States of America 96(22):12731—12736.

[44] Chanas, S.A., Jiang, Q., McMahon, M., McWalter, G.K., McLellan, L.I., Elcombe, C.R., et al., 2002. Loss of the Nrf2 transcription factor causes a marked reduction in constitutive and inducible expression of the glutathione S-transferase Gsta1, Gsta2, Gstm1, Gstm2, Gstm3 and Gstm4 genes in the livers of male and female mice. Biochemical Journal 365(Pt 2):405—416.

[45] Lamsa, V., Levonen, A.L., Sormunen, R., Yamamoto, M., Hakkola, J., 2012. Heme and heme biosynthesis intermediates induce heme oxygen-ase-1 and cytochrome P450 2A5, enzymes with putative sequential roles in heme and bilirubin metabolism: different requirement for transcription factor nuclear factor erythroid- derived 2-like 2. Toxicological Sciences 130(1):132—144.

[46] Cho, H.Y., Miller-DeGraff, L., Blankenship-Paris, T., Wang, X., Bell, D.A., Lih, F., et al., 2019. Sulforaphane enriched transcriptome of lung mitochon-drial energy metabolism and provided pulmonary injury protection via Nrf2 in mice. Toxicology and Applied Pharmacology 364:29—44.

[47] Lazaro, I., Ferre, R., Masana, L., Cabre, A., 2013. Akt and ERK/Nrf2 activation by PUFA oxidation-derived aldehydes upregulates FABP4 expression in human macrophages. Atherosclerosis 230(2):216—222.

[48] Muller, M., Banning, A., Brigelius-Flohe, R., Kipp, A., 2010. Nrf2 target genes are induced under marginal selenium-deficiency. Genes Nutr 5(4):297—307.

[49] Lesniak, W., Szczepanska, A., Kuznicki, J., 2005. Calcyclin (S100A6) expression is stimulated by agents evoking oxidative stress via the antioxidant response element. Biochimica et Biophysica Acta 1744(1):29—37.

[50] Sumi, D., Shimizu, Y., Himeno, S., 2013. Involvement of Nrf2 activation in the upregulation of S100A9 by exposure to inorganic arsenite. International Journal of Molecular Medicine 31(1):259—264.

[51] Hu, R., Xu, C., Shen, G., Jain, M.R., Khor, T.O., Gopalkrishnan, A., et al., 2006. Identification of Nrf2-regulated genes induced by chemopreventive isothiocyanate PEITC by oligonucleotide microarray. Life Sciences 79(20): 1944—1955.